11

Diffraction of monochromatic waves and ultrashort pulses on graphene gratings in a magnetic field

© A.M. Lerer,[1] G.S. Makeeva,[2] I.N. Ivanova,[1] V.I. Kravchenko[1]

[1] Southern Federal University,
344090 Rostov-on-Don, Russia
[2] Penza State University,
440026 Penza, Russia
e-mail: lerer@sfedu.ru

Received December 17, 2025
Revised December 17, 2025
Accepted December 17, 2025

The diffraction of electromagnetic waves on a one-dimensional quasi-periodic diffraction grating formed by graphene ribbons is considered. The magnetic field is applied perpendicular to the substrate plane. Theoretical research is based on the transition using the Poisson transformation from the spectral representation of fields of a periodic grating to the spatial representation of a quasi-periodic one. The rearrangement of the plasmon resonance frequency (PR) by a magnetic field, the rotation of the plane of polarization of the reflected and transmitted waves, and the presence of additional PR are investigated.

Keywords: graphene, metasurface, diffraction grating, antenna array, integral equations, Poisson transform.

DOI: 10.61011/TP.2026.05.63531.336-25

Introduction

The properties of graphene in a magnetic field are well described by the Drude model for plasma in a magnetic field [1]. The elements of the condcitvity matrix $\boldsymbol{\sigma}$ diferent from zero are expressed as follows

$$\sigma_{xx} = \sigma_{yy} = -\frac{2D}{\pi}\, i\, \frac{\omega + i/\tau}{\omega_B^2 - (\omega + i/\tau)^2},$$

$$\sigma_{xy} = -\frac{2D}{\pi}\frac{\omega_B}{\omega_B^2 - (\omega + i/\tau)^2},\ \sigma_{yx} = -\sigma_{xy}, \qquad (1)$$

where ω — cyclic frequency, $D = 2\sigma_0 E_F/\hbar$, $\sigma_0 = 6.08 \cdot 10^{-5}$ S, $\hbar$ — reduced Planck constant, E_F — Fermi energy, $\omega_B = eBv_F^2/E_F$ — cyclic cyclotrone frequency, B — magnetic induction, $v_F = 10^6$ m/s — Fermi velocity, τ — relaxation time. The model error without magnetic field compared to Kubo formula [2] doesn't exceed 5 % up to 25 THz [3].

In the terahertz and near-infrared ranges, the cyclotron frequency ω_B can be equal to the frequency of plasmon resonances, which significantly increases the interaction of the electromagnetic wave with the graphene metasurface. In this regard, a new scientific field has appeared- magneto-plasmonics.

The existence of cyclotron resonance in graphene has been experimentally shown in [4,5], therefore, in the THz and near-infrared regions, the frequency of plasmon resonance [3,5–10], the plane of polarization [8,11] can be adjusted by a magnetic field. One of the widely known structures of graphene meta-surfaces — are diffraction gratings (DG) [9,12].

An effective method for computational modeling of a graphene layer with magnetic displacement in a magnetic field is presented in [13]. The effect of surface conduction anisotropy is modeled and taken into account in the framework of recursive convolution in a finite-difference time domain algorithm (FDTD).

A rigorous analytical method for analyzing the grating of graphene ribbons with magnetic bias is proposed in [14]. The method is based on integral equations describing induced surface currents in a grating of coplanar graphene ribbons. The obtained results predict resonant spectral effects. A closed-form analytical solution for Faraday rotation in graphene ribbons with magnetic bias is obtained.

In [15], the Fourier-based numerical method in the transmission line formulation (TLF) is generalized to analyze multilayer periodic structures based on magnetically biased graphene. The approximate boundary condition proposed for the fast modal Fourier method developed for periodic graphene gratings is modified to analyze such structures.

In [16], an improved wave concept iterative process (WCIP) is outlined for analyzing a new type of tunable graphene connector in the THz range with different physical parameters of graphene. Thanks to a new technique for implementing anisotropic boundary conditions in WCIP method, the anisotropic surface conduction matrix is integrated into this algorithm without using volume discretization. The results of numerical simulation show that the characteristics of the connector can be controlled by changing the chemical potential and magnetic field.

This study comes from the paper [3], where the diffraction phenomenon was theoreticaly analyzed for the periodic graphene DG (Fig. 1). A constant magnetic field directed

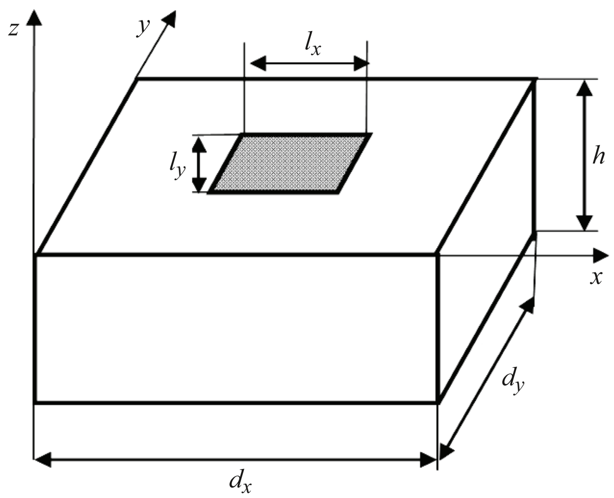

Figure 1. Diffraction grating unit cell.

perpendicular to the plane of the substrate is applied to the DG. The research [3] is based on the numerical and analytical solution of two types of integro-differential equations - paired adders with respect to currents on the strips and volumetric integro-differential ones with respect to the electric field strength inside the strips.

The studied object is a quasi-periodic DG made of a finite number of strips. The method of transition from a two-dimensional periodic DG to a quasi-periodic one is described in [17] — the transition from the spectral representation of fields of a periodic grating to the spatial representation of a quasi-periodic one.

The purpose of the study — modification and verification of method [17] for calculating $1D$, a quasi-periodic DG formed by $(l_y \to \infty)$ graphene ribbons, and studying the Kerr effect — rotation of the plane of polarization when a wave is reflected from DG.

Let the graphene ribbons lie in $z = 0$ plane. Let's denote their surface within the unit cell as S. Figure 1 shows one rectangle, but the number of rectangles in the program is arbitrary. Therefore, S — is a surface of all strips. Let's the density of currents on the strips are denoted as $\mathbf{J}$. Then we can find the electromagnetic field generated by these currents. In particular, [3]:

$$\mathbf{E}(x, y, z) = -iZ_0 \frac{1}{d_x d_y} \sum_{m=-\infty}^{\infty} \sum_{n=-\infty}^{\infty} \mathbf{g}_{mn}(0, z)\mathbf{j}_{mn} \times \exp[i(\alpha_m x + \beta_n y)], \qquad (2)$$

$$\mathbf{j}_{mn} = \int_S \mathbf{J}(x', y')[-i(\alpha_m x' + \beta_n y')]ds', \quad \mathbf{J}(x', y')$$

— density of surface currents on the strips, $\mathbf{g}_{mn}(z, z')$ — terms of the two-dimensional Floquet series of the Green tensor function [3,18],

$$\mathbf{G}(\bar{x}, \bar{y}, z, z') = \frac{1}{d_x d_y} \sum_{m=-\infty}^{\infty} \sum_{n=-\infty}^{\infty} \mathbf{g}_{mn}(z, z') \times \exp[i(\alpha_m \bar{x} + \beta_n \bar{y})], \qquad (3)$$

$\bar{z} = x - x'$, $\bar{y} = y - y'$, $\alpha_m = \frac{2m\pi}{d_x} + k_x$, $\beta_n = \frac{2n\pi}{d_y} + k_y$, k_x, k_y — wave vector components $\mathbf{k}$, Z_0 — vacuum wave impedance.

To move to a finite (non-periodic) grating, you need to (1), (2) replace the Floquet series with Fourier integrals, i.e.

$$\frac{1}{d_x d_y} \sum_{m=-\infty}^{\infty} \sum_{n=-\infty}^{\infty} F(\alpha_m, \beta_n) \to \frac{1}{(2\pi)^2} \int_{-\infty}^{\infty} \int_{-\infty}^{\infty} F(\alpha, \beta) d\alpha d\beta.$$

As a result, we obtain paired integral equations that are solved in a similar way to solving paired summation equations (PSE) [3]. Along with that, two problems arise. First, numerical integration is a more difficult task. We used the simplest rectangle formula, while the integration was reduced to quadrature formulas such as Floquet series (2), (3), but in which d_x, d_y are not periods, but quadrature parameters. At $d_x \gg \lambda$, $d_y \gg \lambda$ quadratures converge quickly. The second problem is more complicated — computer time is proportional to the square of the number of strips in the DG. Therefore, the method from [17] was used to solve this problem.

Let's apply Poisson transform to (2), (3). denote for brevity

$$\mathbf{F}(\alpha_m, \beta_n) = \mathbf{g}_{mn}(0, z)\mathbf{j}_{mn} \exp[i(\alpha_m x + \beta_n y)],$$

$$\mathbf{E}(x, y, z) = -iZ_0 \frac{1}{d_x d_y} \sum_{m=-\infty}^{\infty} \sum_{n=-\infty}^{\infty} \mathbf{F}(\alpha_m, \beta_n) =$$

$$-iZ_0 \frac{1}{d_x d_y} \sum_{m=-\infty}^{\infty} \sum_{n=-\infty}^{\infty} \int_{-\infty}^{\infty} \int_{-\infty}^{\infty} \exp[2\pi i(m\mu + n\nu)] \times \mathbf{F}(\alpha(m), \beta(n), x, y, z) dmdn.$$

After substitution of variables we get

$$\mathbf{E}(x, y, z) = \sum_{\mu=-\infty}^{\infty} \sum_{\nu=-\infty}^{\infty} \exp[-i(\mu k_x d_x + \nu k_y d_y)] \times \mathbf{G}(\mu d_x, \nu d_y), \qquad (4)$$

where

$$\mathbf{G}(\mu d_x, \nu d_y, x, y, z) = \frac{1}{(2\pi)^2} \times \int_{-\infty}^{\infty} \int_{-\infty}^{\infty} \exp[i(\mu d_x \alpha + \nu d_y \beta)] \mathbf{F}(\alpha, \beta) d\alpha d\beta. \qquad (5)$$

From a physical point of view, (2) — is a representation of the diffracted field as a series of spatial harmonics of DG, and (4) —is the sum of the fields diffracted on the strips of each unit cell of the DG. Let's assume in (5) $|\mu| \leq M$, $|\nu| \leq N$. In this case, we obtain an expression for the diffracted field generated by $(2M+1)(2N+1)$ unit cells, assuming that the currents on the strips are the same as those of the infinite DG, i.e., to solve the diffraction problem, the infinite DG with the number of strips placed in one unit cell is still calculated.

The main problem — calculation of integrals in (4) in the far-field zone $kr \to \infty$ For this we use the asymptotics of the integral [19]:

$$\frac{1}{(2\pi)^2}\int\limits_{-\infty}^{\infty}\int\limits_{-\infty}^{\infty} f(\alpha,\beta)\exp(-\gamma|z|)\exp[i(\alpha x+\beta y)]d\alpha d\beta$$

$$\sim ik\cos\theta f(-k\sin\theta\cos\varphi, -k\sin\theta\sin\varphi)\exp[-ikr]\frac{1}{2\pi r},$$

where r, θ, φ — coordinates of the observation point in the spherical coordinate system.

As a result, we'll obtain in the far-field zone

$$E(r,\varphi,\theta) \sim \frac{\exp(-ikr)}{r}\mathbf{\Phi}(\varphi,\theta),$$

where

$$\mathbf{\Phi}(\varphi,\theta) = ik\cos\theta\sum_{\mu=-M}^{M}\sum_{\nu=-N}^{N}$$

$$\times\exp\big[i(\mu d_x(\alpha+k_x)+\nu d_y(\beta+k_y))\big]\tilde{\mathbf{E}}(\alpha,\beta),$$

$\alpha = -k\sin\theta\cos\varphi$, $\beta = -k\sin\theta\sin\varphi$. Far field

$$\Phi_\theta = \cos\theta(\Phi_x\cos\varphi + \Phi_y\sin\varphi) - \Phi_z\sin\theta,$$

$$\Phi_\varphi = -\Phi_x\sin\varphi + \Phi_y\cos\varphi.$$

For the $1D$ DG there's no series in (4)

$$\mathbf{E}(x,z) = \sum_{\mu=-M}^{M}\exp[-i\mu k_x d_x]\mathbf{H}(\mu d_x, x, z),$$

$$\mathbf{H}(\mu d_x, x, z) = \frac{1}{2\pi}\int\limits_{-\infty}^{\infty}\exp[i\mu d_x\alpha]\mathbf{F}(\alpha,x,z)d\alpha.$$

The integral asymptotics is found by the saddle-point method. For the reflected wave

$$I(\kappa r) = \frac{1}{2\pi}\int\limits_{-\infty}^{\infty} f(\alpha)\frac{\exp(i\alpha x-\gamma z)}{\gamma}d\alpha \sim 2if(\alpha_0)\frac{1}{\sqrt{kr\pi}}$$

$$\times\exp\Big(-ikr+i\frac{\pi}{4}\Big),$$

where $\gamma = \sqrt{\alpha^2-k^2}$, $r = \sqrt{x^2+y^2}$, $\alpha_0 = -k\sin\theta$, $f(\alpha) = \kappa\exp[i\mu d_x\alpha]\tilde{\mathbf{E}}(\alpha)$.

In this paper, we present the results for the reflection of a wave from the one-dimensional periodic DGs, in which $l_y \to \infty$. The plane of incidence is perpendicular to graphene ribbons — $\varphi = 0$ Designations of polarization of the incident wave as in optics: p-polarization — electrical field intensity vector $\mathbf{E}(x,z)$ is perpendicular to the graphene ribbons, and vector $\mathbf{H}(x,z)$ is parallel to them, s-polarization — vector $\mathbf{H}(x,z)$ is perpendicular to the graphene ribbons, vector $\mathbf{e}(x,z)$ is parallel to them. In the absence of a magnetic field in $1D$ DG, the reflected and transmitted waves do not change their polarization.

Substrate parameters — layer with a thickness of $100\,\mu$m with reflection index $n = 1.5$, semi-infinite dielectric with $n = 1.77$. Width of the graphene ribbons $l_x = 40\,\mu$m. Graphene parameters (except for Fig. 4) $E_F = 0.25$ eV, $\tau = 1$ ps.

To compare the diagrams of light scattering (DLS) with a different number of N strips, the figures show the values of Φ/N.

Fig. 2 shows comparison of the two methods of calculation of reflected fields in the far zone $1d$ of DG, p – polarization. Distance between the centers of ribbons — $d_x = 50\,\mu$m, incidence angle 30°, $B = 0.5$ T, frequency $f = 1$ THz is selected close to the plasmon resonance frequency of the infinite DG. Φ_x — DLS component in the incidence plane, and Φ_y in orthogonal plane. Φ_y are normalized to the maximum of DLS of the main polarization.

Fig. 2 shows that even for the 5-ribbon DG, the two methods for calculating the directional patterns of the final DG are close, and for the 11-ribbon DG, they practically coincide. It should be noted that the order of SLAE (system of linear algebraic equations) in the first method is, N times greater than in the second. Therefore, the results of calculations given in Fig. 6–8, were obtained by the second method.

Fig. 3, 4 illustrate the results for the infinite DG with a period $d = 50\,\mu$m at two levels of Fermi energy. Figures in the left — s-polarization of the incident wave, in the right — p-polarization. Solid lines — components of the electric field strength, the direction of which coincides with the direction of the vector of the electric field strength of the incident wave, dashed lines — cross-polarization. The amplitude of the incident wave is assumed to be one. Incident angle 55°. Digits in the curves — values of B, [T]. It can be seen that the angle of rotation of the polarization plane of the reflected wave is greater for p polarization, which has a plasmon resonance of the cross current. For s polarization, the cross current also appears in the magnetic field of DG, but the plasmon resonance is weakly expressed. Parameter φ — shift phase between E_x and E_y. The reflected wave is elliptically polarized. By changing the value of E_F, B, circular polarization of the reflected wave can be achieved. At $B = 0$, $\sigma_{xx} = \sigma_{yy}$ and, consequently, the frequency of the plasmon resonance decreases with the decline in E_F (1). At $B \neq 0$ a parallel process occurs — increase of the cyclotronic frequency ω_B.

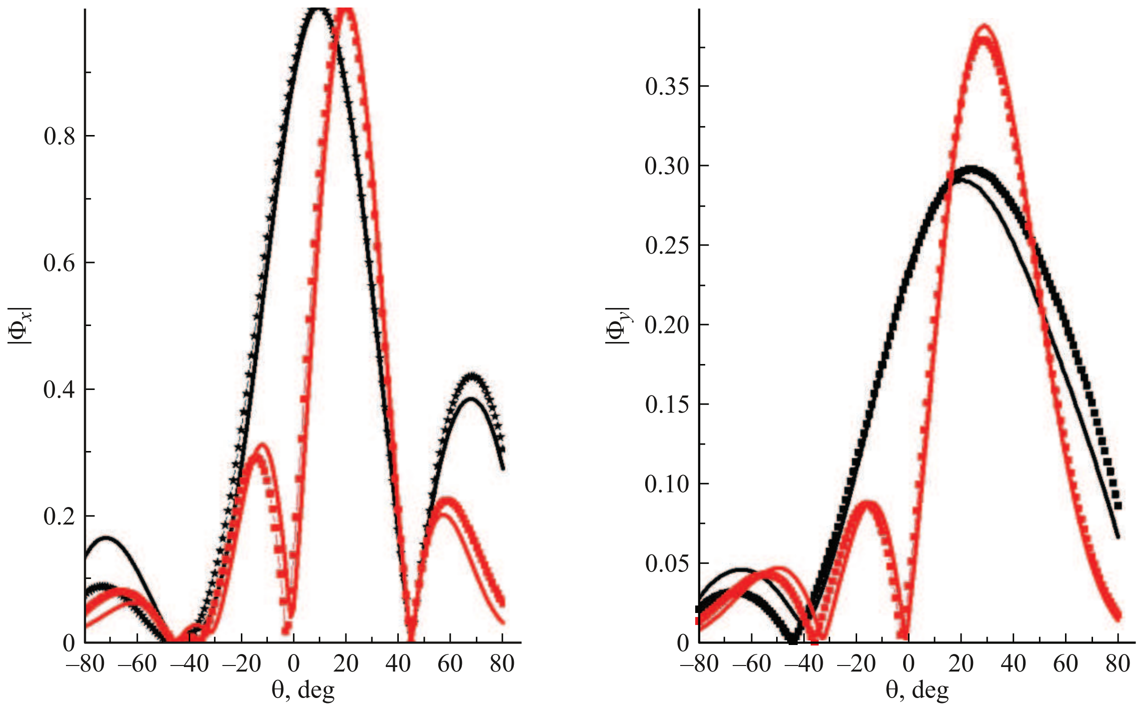

Figure 2. Two calculation methods compared. Number of ribbons $N = 5$ (black curves) and $N = 11$ (red curves. Lines without symbols — first method, with symbols — second method.

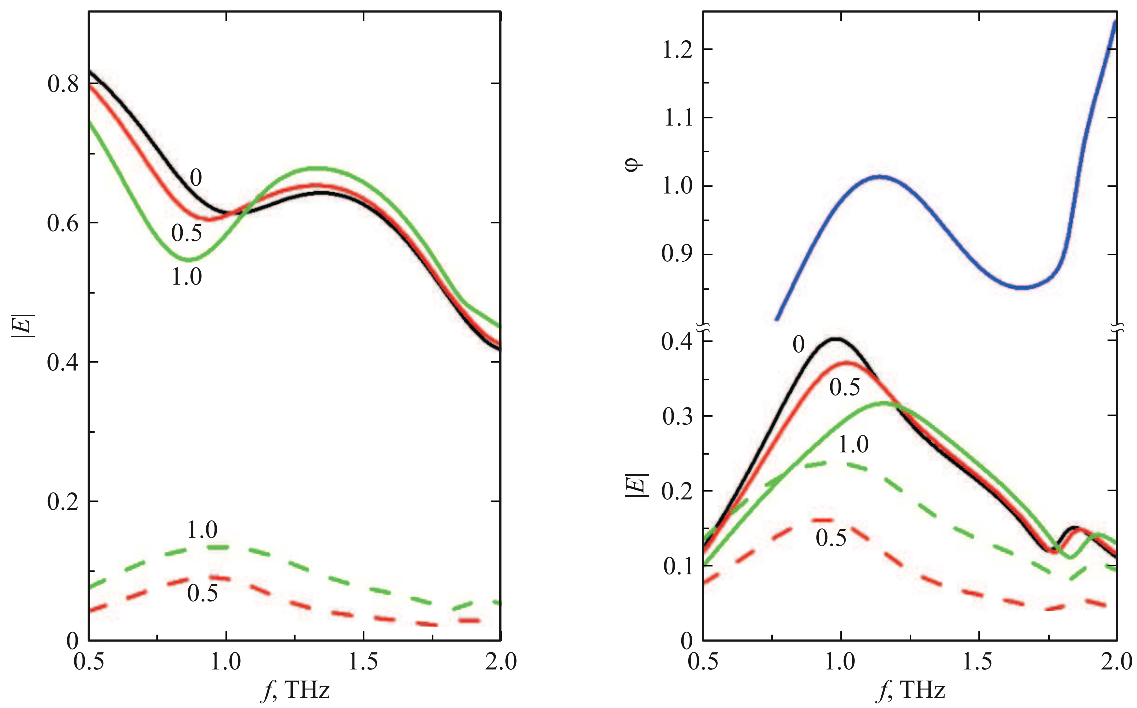

Figure 3. The amplitude of the wave reflected from the periodic DG. $E_F = 0.25$ eV.

Fig. 5–7 shows the results for diffraction of only *p*-polarized wave. The angle of incidence 55° (except for Fig. 8) is close to Brewster angle, equal 56○. In all figures of the reflected wave DLS, the figure on the left — Φ_x in the plane of incidence, on the right — Φ_y in the perpendicular plane. The spacing between the strips centers was $d_x = 80\,\mu$m.

Figure 5 illustrates rotation of the polarization plane of a reflected wave when exposed to magnetic field. The selected frequency is close to the plasmon resonance fre-

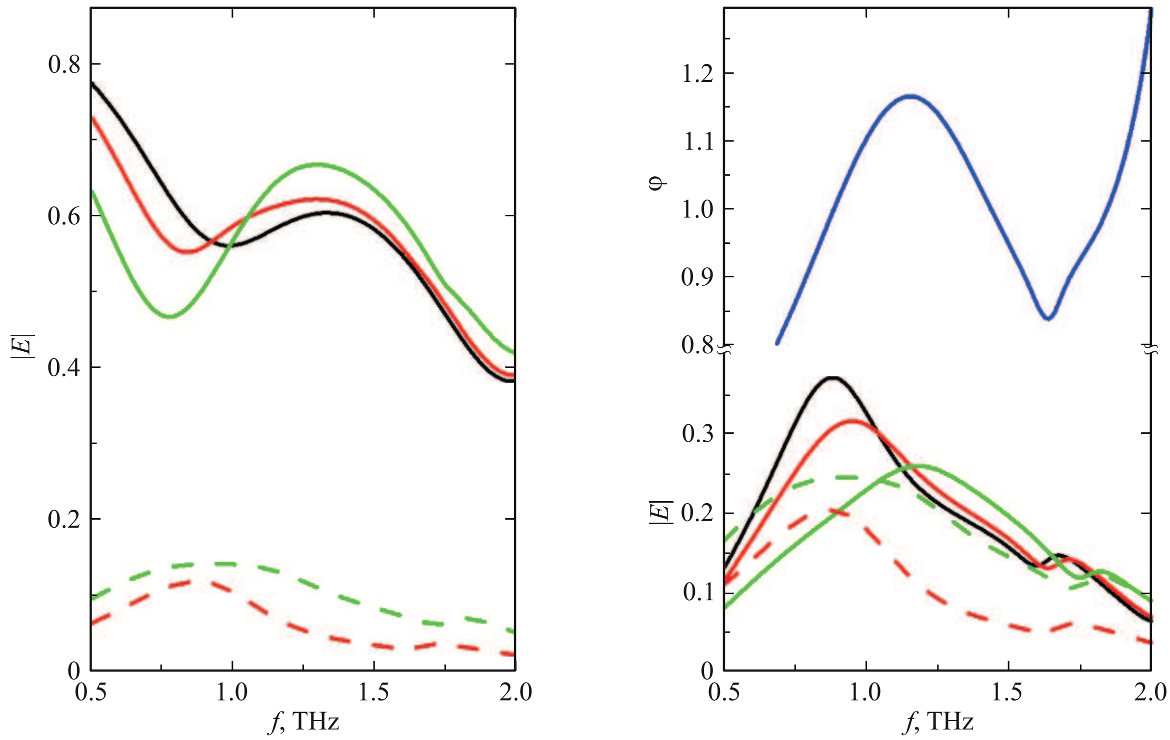

Figure 4. The amplitude of the wave reflected from the periodic DG. $E_F = 0.2$ eV. The curves are designated similar those in Fig. 3.

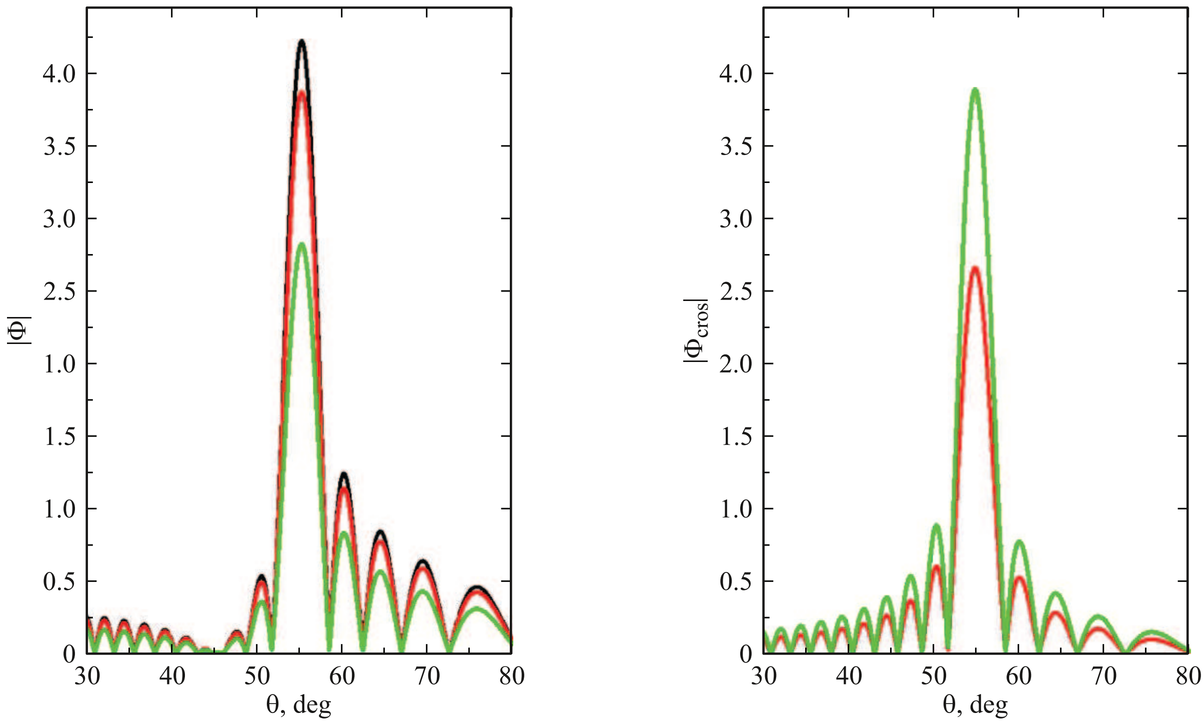

Figure 5. Scattering diagram of DG in 101-th strip at various B, T: 0 — black, 0.5 — red, 1 — green curves. $f = 1.1$ THz.

quency $f_p = 1.12$ THz at $B = 0.5$ T. A growth of magnetic induction naturally decreases the field component in the plane of incidence and increases it in the perpendicular plane.

At magnetoplasmic resonance frequency, there's maximum angle of rotation of the polarization plane (Fig. 6, 7). Interestingly, the frequency shift to the right from f_p reduces the cross-polarization. An increase in the number

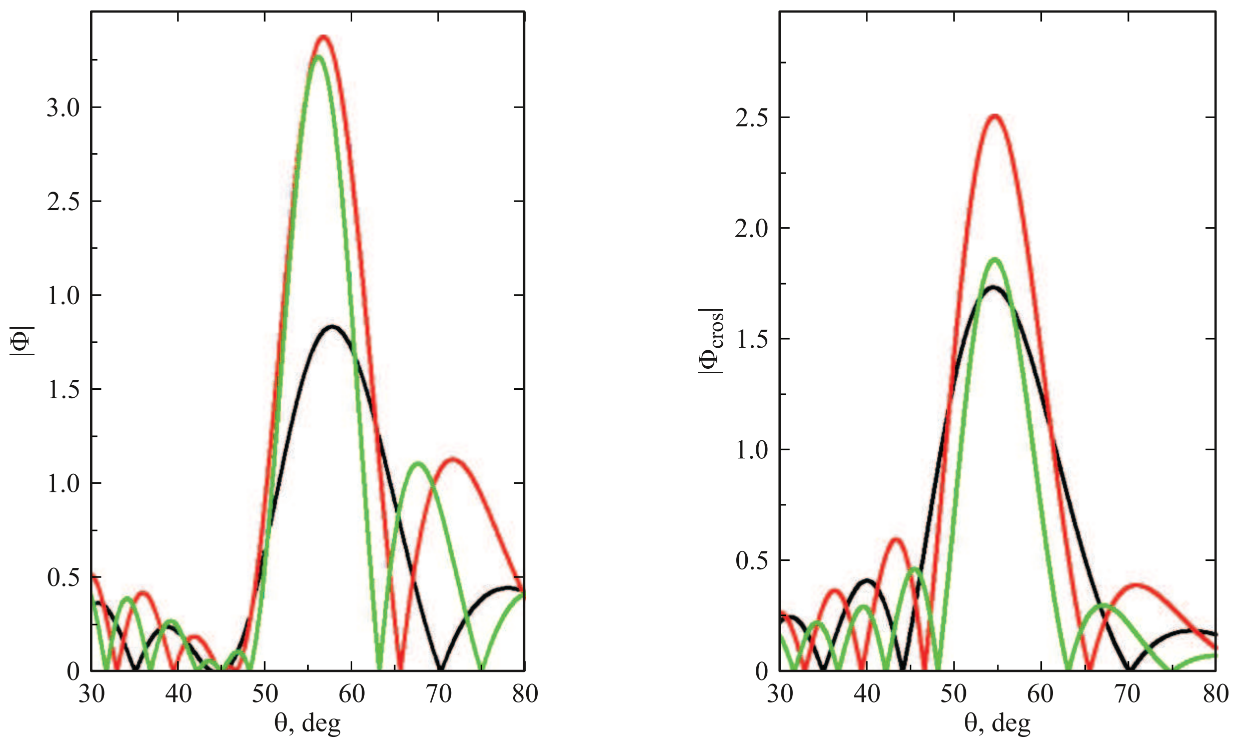

Figure 6. The scattering diagram of the DG from the 41st strip at different frequencies. $B = 0.5\,\mathrm{T}$. f, THz: 0.75 — black, 1.0 — red, 1.25 — green curves. $d_x = 80\,\mu$m.

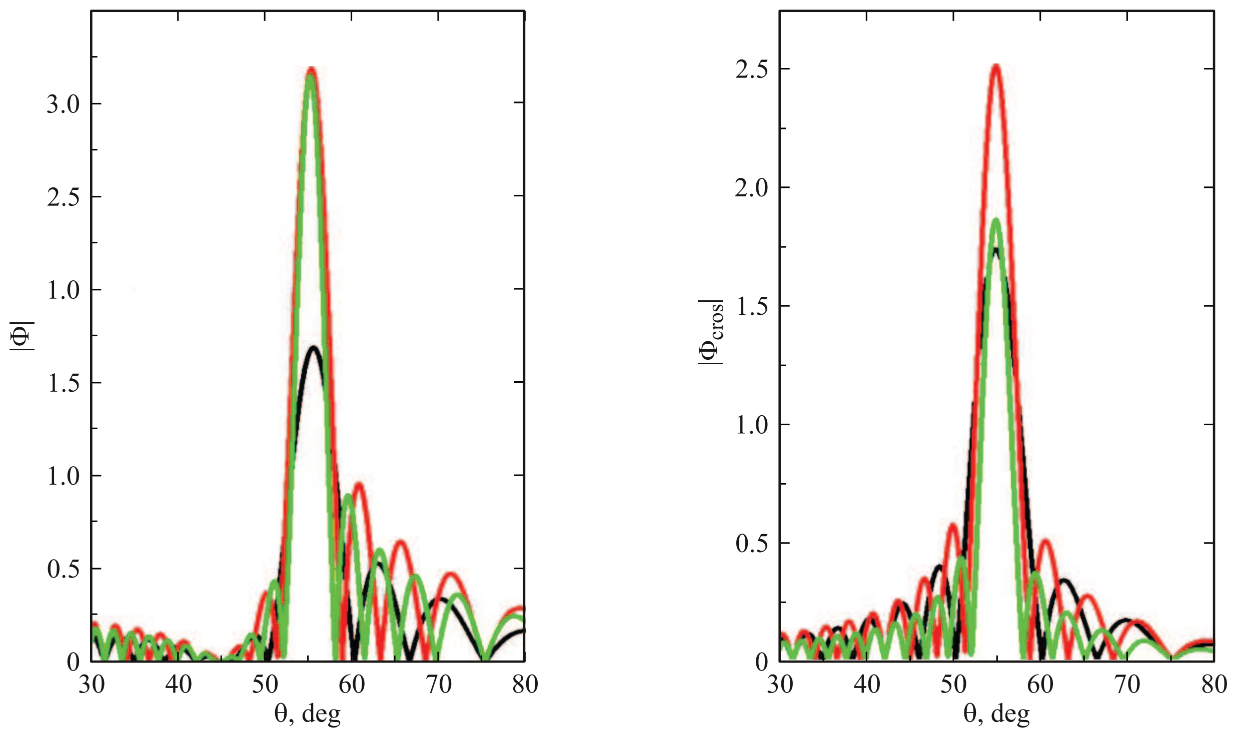

Figure 7. The scattering diagram of the DG from the 101-st strip at different frequencies. $B = 0.5\,\mathrm{T}$. f, THz: 0.75 — black, 1.0 — red, 1.25 — green curves. $d_x = 80\,\mu$m.

of ribbons has little effect on the normalized value Φ_x and Φ_y, but, naturally, narrows DLS and brings the reflection angle (i.e., the maxima of Φ_x and Φ_y) closer to the angle of incidence.

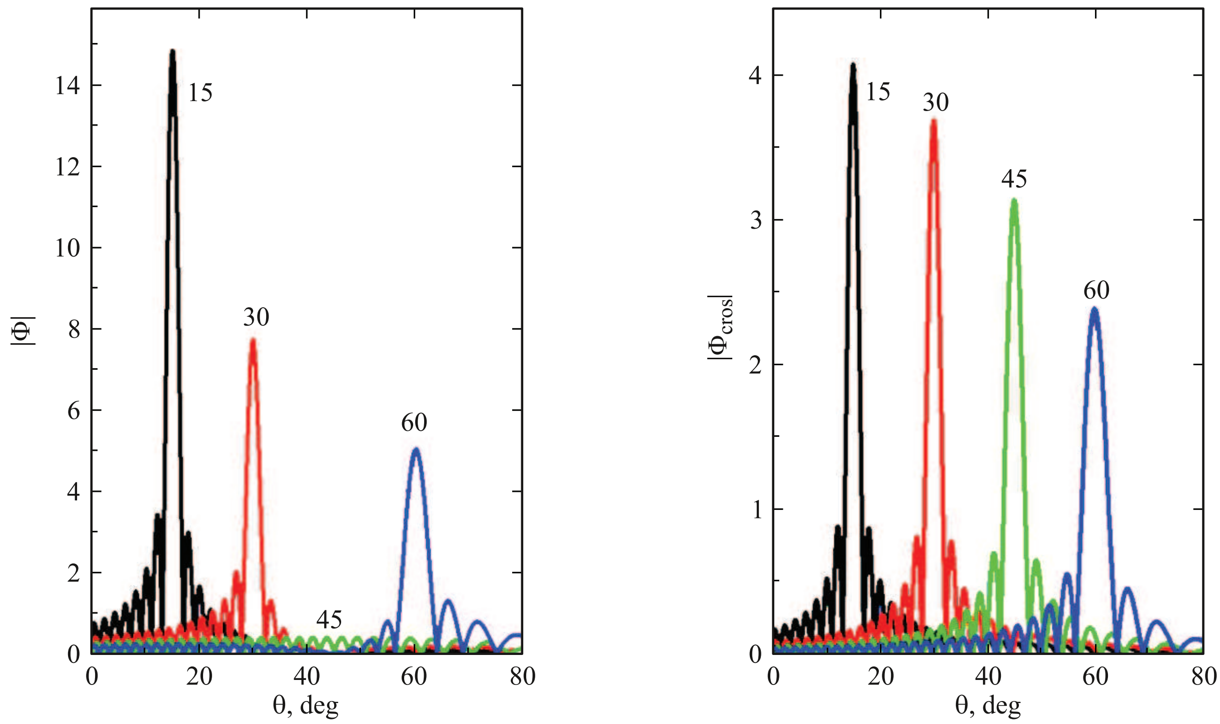

Figure 8. The scattering diagram of the DG from the 101-st strip at different angles of incidence. $f = 1.1$ THz. $B = 0.5$ T. $d_x = 80\,\mu$m. Digits on curves — incident angles in degrees.

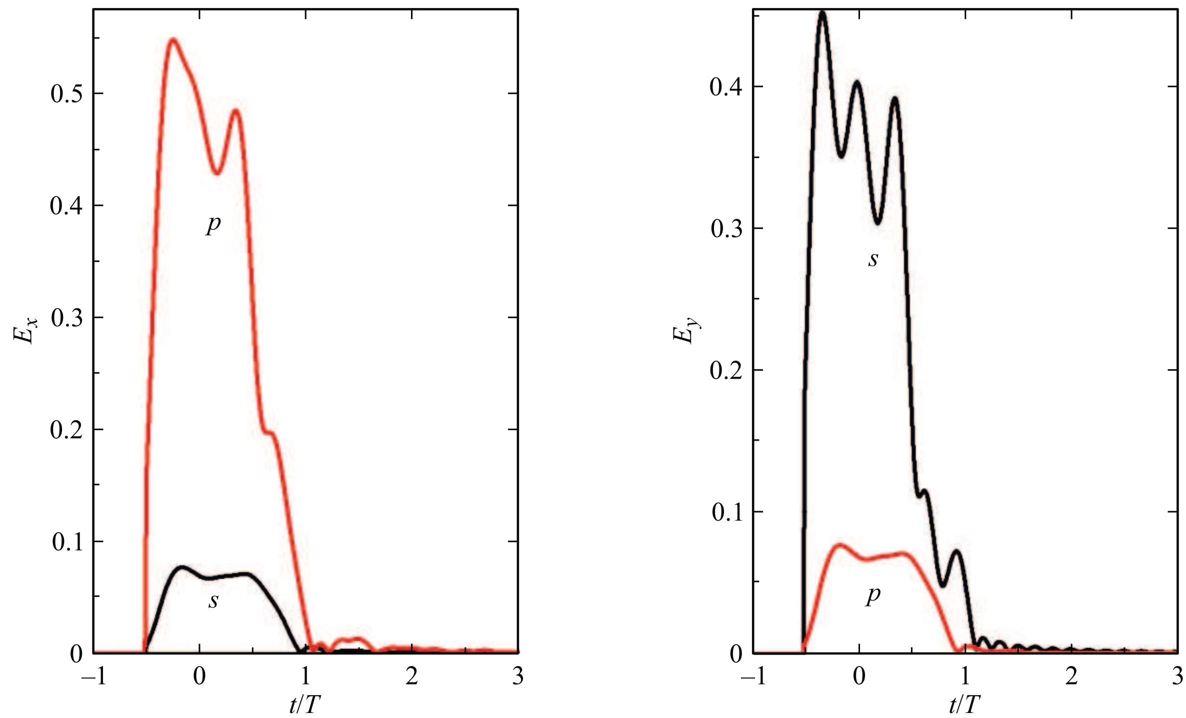

Figure 9. Reflection of a rectangular EMR from the infinite DG with a period of $d_x = 50\,\mu$m. Carrier frequency $f_0 = 1.6$ THz, $T = 2$ ps. $B = 0.5$ T.

The angle of rotation of the polarization plane of the reflected wave Φ_y/Φ_x greatly depends on the angle of incidence (Fig. 8). If Φ_y rises smoothly as the angle increases, then Φ_x first decreases due to rotation of polarization plane, at the angle of incidence 45° $\Phi_x \approx 0$, then Φ_x starts to grow.

Apart from the diffraction of a monochromatic wave, the diffraction of electromagnetic pulses, the duration of which is several periods of oscillation of the carrier, was also studied. The problem's solution was associated with the frequency domain. Due to the strong dependence of the reflection coefficient, there is naturally a strong distortion of the pulse (Fig. 9).

Conclusions

1. The solution of the boundary value problem of plane electromagnetic wave diffraction on a periodic diffraction grating based on graphene ribbons in a magnetic field was obtained by two methods:

— in the first method — PSE were solved where the unknown function was current density in the graphene ribbons;

— in the second method, an integro-differential equation with respect to the electric field strength inside graphene strips was solved.

2. For DG with a finite number of ribbons in the formulas obtained, the Floquet series shall be replaced by Fourier integrals.

3. When calculating the DG with a large number of ribbons, a transition was made using the Poisson transform from the spectral representation of the fields of a periodic grating to the spatial representation of a quasi-periodic one. The asymptotics in the far-field zone was obtained.

4. The method outlined in this paper can be extended to analyze and design other tunable terahertz non-interchangeable devices, such as insulators, circulators, phase shifters, and switches [20]. The findings may have potential applications in the design of magnetic field sensors and tunable devices based on the Kerr effect [21].

Funding

The study was supported by the Ministry of Science and Higher Education of the Russian Federation (State assignment in the field of research. project No. FENW-2023-0010/GZ0110/23-11-IF).

Conflict of interest

The authors declare that they have no conflict of interest.

References

[1] W.H. Wang S.P. Apel, J.M. Kinaret. Phys. Rev. B, **86**, 125450 (2012).

[2] G.W.J. Hanson. Appl. Phys., **103** (6), 064302 (2008).

[3] A.M. Lehrer. Radiotekhnika i elektronika, **69** (11), 17 (2024) (in Russian).

[4] M. Tamagnone, T.M. Slipchenko, C. Moldovan, P.Q. Liu, A. Centeno, H. Hasani, A. Zurutuza, A.M. Ionescu, L. Martin-Moreno, J. Faist, J.R. Mosig, A.B. Kuzmenko, J.-M. Poumirol. Phys. Rev. B, **97**, 241410 (2018). DOI: https://doi.org/10.1103/PhysRevB.97.241410

[5] M.L. Chin, S. Matschy, F. Stawitzki, J. Poojali, H.A. Hafez, D. Turchinovich, S. Winnerl, G. Kumar, R.L. Myers-Ward, M.T. Dejarld. J. Phys.: Photon., **3**, 01LT01 (2021). DOI: 10.1088/2515-7647/abd7d0

[6] D.A. Kuzmin, I.V. Bychkov, V.G. Shavrov, V.V. Temnov. Nanophotonics, **7** (3), 597 (2018). DOI: 10.1515/nanoph-2017-0095

[7] W. Ningning, D. Linhui, W. Weihua. Phys. Rev. B, **108** (8), 085406 (2023).

[8] Zh. Zesen, G. Zhilong, C. Lei. J. Phys. D: Appl. Phys., **56**, 365104 (2023). DOI: 10.1088/1361-6463/acda45

[9] J.-Q. Liu, Yu-X. Zhou, L. Li, P. Wang, A.V. Zayats. Optics Express, **23** (10), 12525 (2015). DOI: 10.1364/OE.23.012524

[10] Y. Lu, Ch. Wang, Sh. Zhao, Y. Wen. Frontiers Phys., **8**, 622839 (2021). DOI: 10.3389/fphy.2020.622839

[11] P. Padmanabhan, S. Boubanga-Tombet, H. Fukidome, T. Otsuji, R.P. Prasankumar. Appl. Phys. Lett., **116**, 221107 (2020). DOI: 10.1063/5.0006448

[12] T. Guo, C.J. Argyropoulos. Appl. Phys., **134**, 050901 (2023). DOI: 10.1063/5.0152664

[13] S.A. Amanatiadis, N.V. Kantartzis, T. Ohtani, Y. Kanai. IEEE Transactions on Magnetics, **54** (3), 1, 7201504 (2018). DOI: 10.1109/TMAG.2017.2749558

[14] M. Rahmanzadeh, B. Rejaei, M. Memarian. arXiv:1908.04571v1 [physics.optics] https://doi.org/10.48550/arXiv.1908.04571

[15] P.K. Khoozani, M. Maddahali, M. Shahabadi, A. Bakhtafrouz. J. Optical Society of America B, **33** (12), 2566 (2016). https://doi.org/10.1364/JOSAB.33.002566

[16] A. Hlali, Z. Houaneb, H. Zairi. IEEE Transactions on Magnetics, **56** (8), 1–8, 2800308 (2020). DOI: 10.1109/TMAG.2020.3000669

[17] A.M. Lehrer, I.N. Ivanova, V.V. Makhno. Antenny, **3**, 76 (2021) (in Russian).

[18] A.M. Lehrer, G.S. Makeeva, V.V. Cherepanov. Radiotekhnika i elektronika, **66** (6), 543 (2021) (in Russian).

[19] A.M. Lehrer, G.P. Sinyavsky. Vestnik MGU. Seriya 3, **6**, 48 (2010) (in Russian).

[20] I. Mazraeh-Fard, A. Alighanbari. Appl. Optics, **62** (30), 8042 (2023). https://doi.org/10.1364/AO.497603

[21] B. Roumi, R. Abdi-Ghaleh. Phys. E: Low-dimensional Systems and Nanostructures, **144**, article id. 115445 (2022). https://doi.org/10.1016/j.physe.2022.115445

Translated by T.Zorina